Effect of Coiling Temperature on Bainite Transformation in Hot-Rolled Automotive Sheet Steel


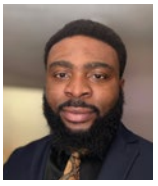



Advanced high-strength steel (AHSS) is used extensively in automotive applications for its excellent formability, high strength with weight-reduction capacity and improved crashworthiness. An industrially processed as-cast AHSS slab sample (0.3C, 2.0Si, 2.5Mn) was hot rolled after being fully austenitized at 1,200°C, followed by isothermal holding to simulate coiling temperature ranging from 500°C to 600°C for 24 hours, and later air cooled to room temperature. Bainite transformation was studied at subcritical temperature during coiling of AHSS sheet. A mixture of ferrite, bainite and retained austenite was evident in the hot-rolled microstructure. The effect of different coiling temperatures on morphology and mechanical properties (tensile, hardness, cold rollability) is discussed.

Authors

Barshan Saha (top left), Graduate Research Assistant, Peaslee Steel Manufacturing Research Center, Department of Materials Science and Engineering, Missouri University of Science and Technology, Rolla, Mo., USA
barshan.saha@mst.edu

Henry Haffner (top center), Department of Mechanical and Aerospace Engineering, Missouri University of Science and Technology, Rolla, Mo., USA
hahxhz@mst.edu

Mario F. Buchely (top right), Roberta and G. Robert Couch Assistant Professor, Peaslee Steel Manufacturing Research Center, Department of Materials Science and Engineering, Missouri University of Science and Technology, Rolla, Mo., USA
buchelym@mst.edu

Simon Lekakh (bottom left), Professor, Peaslee Steel Manufacturing Research Center, Department of Materials Science and Engineering, Missouri University of Science and Technology, Rolla, Mo., USA
lekakhs@mst.edu

K. Chandrashekhara (bottom center), Curators' Distinguished Professor of Mechanical and Aerospace Engineering, Department of Mechanical and Aerospace Engineering, Missouri University of Science and Technology, Rolla, Mo., USA
chandra@mst.edu

Ronald O'Malley (bottom right), F. Kenneth Iverson Chair and Professor for Steelmaking Technologies and Director, Peaslee Steel Manufacturing Research Center, Department of Materials Science and Engineering, Missouri University of Science and Technology, Rolla, Mo., USA
omalleyr@mst.edu

Introduction

Advanced high-strength steels (AHSS) represent a unique class of materials engineered to achieve an exceptional combination of high strength, ductility and toughness.[1,2] They are considered ideal for application requiring lightweight yet durable components. Therefore, AHSS is predominantly utilized in automotive manufacturing to enhance fuel efficiency for its excellent high strength with respect to weight. Moreover, AHSS provides the superior strength-ductility balance demanded by the car industry to ensure better crash safety as well as stiff body parts.

AHSS steels have different groups of subgroups depending on alloying elements and the existing microstructures. Among them, dual-phase (DP), multiphase (MP) bake-hardening (BH), transformation-induced plasticity (TRIP) steel, twinning-induced plasticity (TWIP) steel, etc.[2,3] Since TRIP and TWIP steels change their strength during forming, their properties are controlled by both chemistries and the rolling parameters (hot rolling, cold rolling). The microstructure of the final products is usually characterized by martensitic and bainitic microstructure fractions which result in higher strength with good formability. However, this research will study exclusively the hot rolling parameters to produce hot-rolled product having improved cold rolling ability.[3,4]

The main alloying elements of AHSS steels are C, Mn, Si, Nb, V, Ti, etc. Typically, carbon is held within 0.1–0.3%, whereas Mn and Si levels are typically higher than those found in high-strength low-alloy (HSLA), structural-grade steels to increase strength

and formability. Mn ranges from 1.5 to 2.5%, which acts as an austenite stabilizer to retard ferrite formation.[3,5,6] Also, Mn enhances hardenability of the steel by allowing control of the formation of multiphase microstructures like martensite and bainite, which is desired in AHSS. On the other hand, Si is a ferrite stabilizer that promotes ferritic transformation responsible for formability. In addition, microalloying elements like Nb, Ti form stable carbonitrides to inhibit grain growth and refine microstructure.[4,7,8]

Mechanical properties such as strength and ductility are predominantly determined by the microstructure, which can be influenced by hot rolling and subsequent heat treatments like annealing, normalizing, tempering, quenching, etc. The purpose of hot rolling is to achieve a geometry within tolerance for the application and transform coarse as-cast microstructure into a homogeneous wrought microstructure to ensure better mechanical properties. Hot rolling parameters such as final rolling temperature (FRT), cooling rate after hot rolling, coiling temperature (CT), etc., impact the ferrite, pearlite and bainitic transformation.[9,10] For subsequent cold rolling, coiling temperature and self-tempering play a significant role in the phase transformation and final properties.[4] Higher coiling temperature (600–700°C) after hot rolling produces a softer ferrite-pearlite microstructure, which makes the material easier to process in the cold rolling mill, whereas lower coiling temperature (~450–500°C) promotes harder bainitic morphology, which requires higher forces for cold rolling but leads to more homogeneous and fine-grained microstructures with improved strength. Therefore, an understanding of the bainite transformation during coiling is necessary for designing better annealing cycles with improved cold rollability without compromising mechanical properties.[11,12] In this research, thermomechanical processing using a lab-scale hot rolling mill and quenching dilatometer, coupled with experimental and theoretical data analysis with JMatPro and MATLAB, and characterization by optical microscopy (OM), scanning electron microscopy (SEM) was performed to study the effect of coiling temperature on the bainite transformation in hot-rolled materials of AHSS sheets for automotive applications.

Experimental Procedure

Industrially processed AHSS slabs were used in this study. The chemical composition of this steel grade is presented in Table 1. The material was obtained from a thin-slab caster in an as-cast condition. After sectioning and grinding, cylindrical samples of 3 mm (~0.12 inch) × 10 mm (~0.39 inch) were extracted from the 1/4 (quarter) thickness section of the slab using a Maxiem 707 water-jet cutter. The whole process flowchart is shown in Fig. 1.

Cylindrical samples were characterized by quenching dilatometry to obtain the phase transformation in this material. The Linseis DIL L78 Rita quenching dilatometer was used for this purpose. During dilatometry test, the cylinders were held at 1,200°C for 2 minutes to austenitize the sample, followed by holding at 1,000°C for 1 minute to homogenize the system before controlled cooled to room temperature at 10°C/second, 1°C/second and 0.1°C/second. A schematic of the heat and cooling cycle is shown in Fig. 2a. For minimizing oxidation on the surface of the sample, the whole experiment was performed under a high-purity helium gas atmosphere for faster cooling rate (10°C/second) and high-purity argon gas atmosphere for slower cooling rate (1°C/second, 0.1°C/second). After the completion of dilatometry, the pin sample was cross-sectioned and polished for observing microstructure in an OM.

Concurrently, 75-mm (~3 inches) x 50-mm (~2 inches) x 25-mm (1 inch) rectangular sections were cut from the slab and surface ground for hot rolling. The rolling specimen was wrapped with stainless steel foil to protect its surface from decarburization at high temperature. The sample was austenitized at 1,200°C for 1 hour in a silicon carbide (SiC) furnace, followed by multipass rolling at 1,200°C using a lab-scale STANAT rolling mill equipped with 5-inch-diameter rolls in a 2-high configuration. After each pass, the sample was transferred to a SiC furnace to regain the desired hot rolling temperature (1,200°C). The thermal cycle of the hot rolling process is shown in Fig. 2b. The thickness reduction percentages for each rolling pass along with other rolling parameters are shown in Table 2. After completing eight rolling passes, a sample with a final thickness of 4 mm was transferred to electric box furnace (EBF) and held isothermally for 24 hours to complete the phase transformation at different simulated coiling temperatures (600°C, 550°C, 500°C). The isothermal holding temperature was chosen to mimic the coiling temperatures employed in production after hot rolling. After soaking for 24 hours, the samples were air-cooled to room temperature.

Once the rolled sample reached room temperature, water-jet cutting was utilized to extract tensile coupon specimens of 25-mm gauge length and 4-mm thickness.

Table 1

Chemical Composition of Industrially Processed Advanced High-Strength Steel (AHSS) Grade Specimen

C	Mn	Si	Al	Nb	Ti	N
0.20–0.30	1.50–2.50	0.50–2.00	0.50–1.00	<0.05	<0.05	<0.05

Figure 1

Process flowchart of experimental procedure.

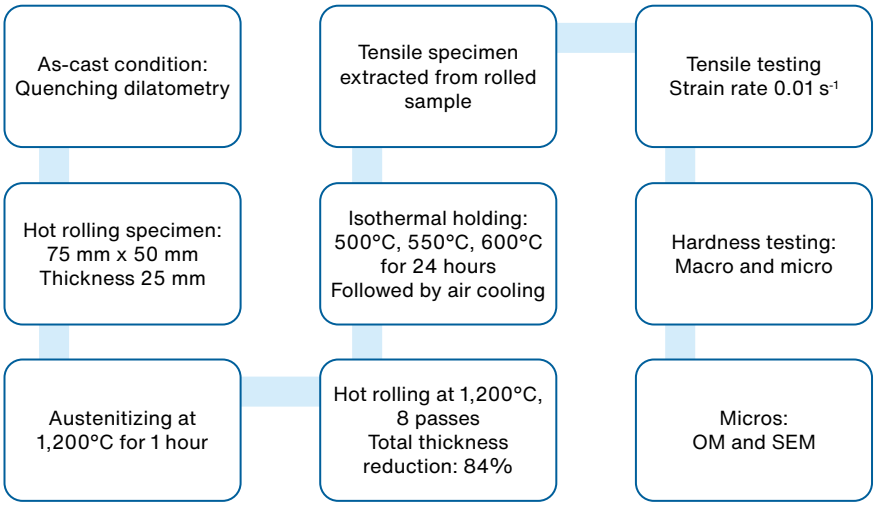

A 250 kN MTS test frame with laser extensometer was used to perform the tensile testing of the as-cast and three specimens with different hot-rolled conditions. The strain rate used for tensile testing was set 0.01 second^{-1}. The laser extensometer was used to capture the continuous displacement of the specimen during the experiment. Later, the stress-strain curve was plotted in MATLAB using the experimental force and displacement data. In addition, both Rockwell hardness and Vickers microhardness of as-cast and as-rolled specimens were measured. The characterization of hot-rolled specimens was also performed using OM and scanning electron microscope (TESCAN SEM).

Results and Discussion

Phase Prediction Using JMatPro Simulation

Fig. 3 shows phase predictions upon cooling for the AHSS sample using JMatPro Version-14.0 software and the general steel database. According to these predictions, the phases at room temperature were predicted to be a mixture of ferrite and cementite under equilibrium conditions. Among the major phases (Fig. 3a), ferrite started to form at ~850°C during cooling from fully austenite region. The volume fraction of ferrite increased with the decrease of temperature. The remaining austenite was fully transformed into ferrite and cementite at ~690°C.

Apart from the major phases like ferrite and cementite, Nb, Ti nitrides ((Nb, V) N), manganese sulfide (MnS), Nb, Ti carbonitrides (Nb, Ti -(C, N)) were also predicted (Fig. 3b). Microalloying elements like Nb, Ti forms complex metal nitrides and carbonitrides that can act as a grain growth inhibitor in AHSS grades.

Continuous Cooling Transformation (CCT) and Time-Temperature Transformation (TTT) Simulation

Fig. 4 shows continuous cooling transformation (CCT) obtained by JMatPro using bulk composition shown in Table 1, and assuming a prior austenitic grain size of

Figure 2

Thermomechanical processes: Thermal cycle of quenching dilatometry (a), and thermal cycle of hot rolling process (b).

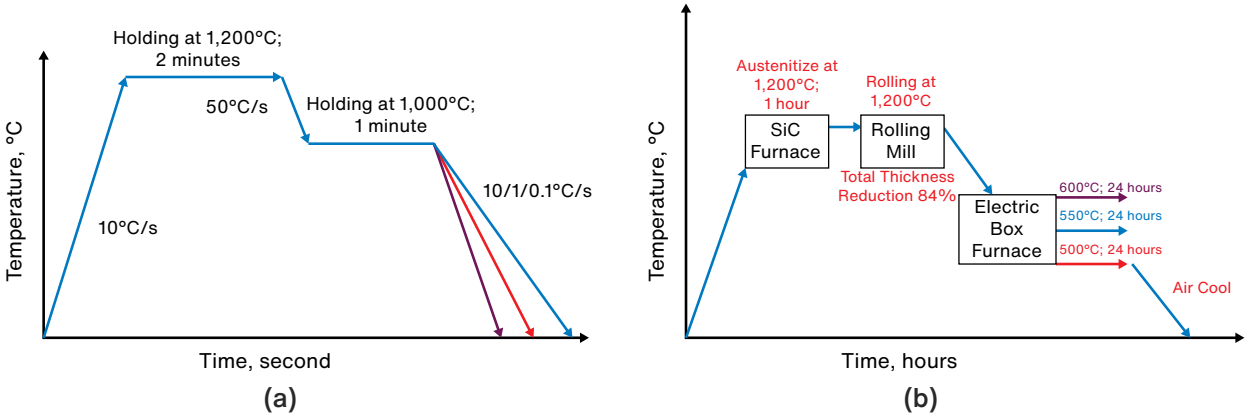

Figure 3

JMatPro predictions using bulk chemistry: Major phases (a), minor phases (b).

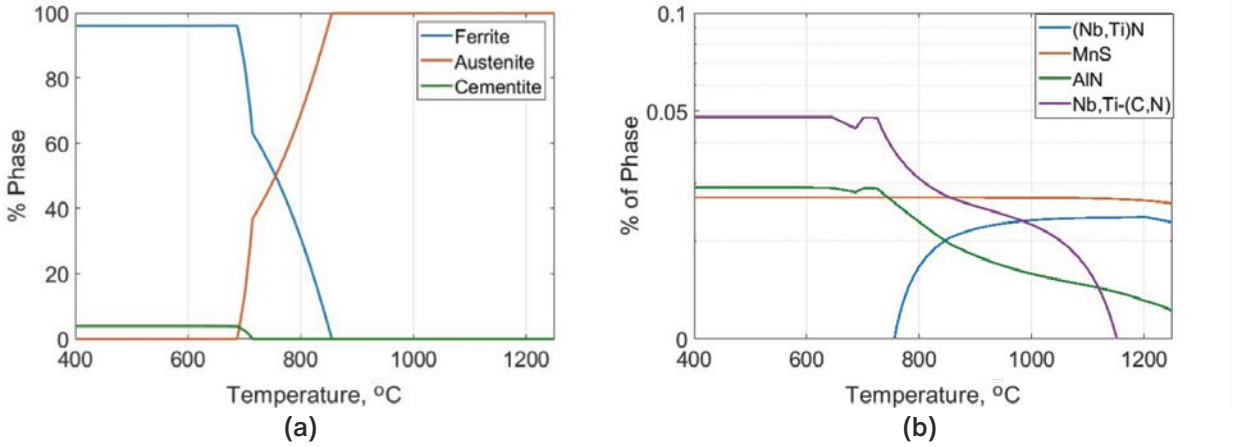

100 µm. It is evident that at cooling rates higher than 10°C/second, a fully martensitic microstructure results, whereas a mixture of bainite and ferrite is observed at 10°C/second. The presence of pearlite starts to become visible at around 1°C/second and slower cooling rates. Some bainite is observed in every cooling condition below 10°C/second.

Fig. 5 shows time-temperature transformation (TTT) obtained by JMatPro using bulk composition shown in Table 1, and assuming a prior austenitic grain size of 100 µm. The ferrite, pearlite, bainite nose is shifted to the left compared to the CCT.

Dilatometric Results

JMatPro can also be used as a simulation tool to obtain a dilatometric plot (temperature versus linear expansion). Fig. 6a shows the length change upon cooling predicted by JMatPro. The change of slope at certain temperatures denotes a specific phase transformation. Likewise, the slope change at around 500°C is related to bainite transformation and at around 350°C is related to the martensitic transformation.

Fig. 6b shows the experimental dilatometric curves for three cooling conditions (10°C/second, 1°C/second and 0.1°C/second). Comparing experimental and simulated results, a discrepancy of transformation temperature is observed in intermediate cooling rates of 1°C/second and 0.1°C/second. Even though in Fig. 6c both JMatPro and dilatometry showed the martensitic transformation occurred at ~350°C, a difference between bainite, ferrite and pearlite transformations in experimental and simulated results is apparent in Figs. 6d and 6e.

The simulation results shown in Fig. 6d predict ferrite transformation at ~750°C and the bainite transformation at ~450°C. However, quenching dilatometry determined the bainite transformation at ~550°C and the martensite start at ~350°C, which was not predicted to form in the simulation.

Figure 4

Continuous cooling transformation (CCT) plot from JMatPro Simulation.

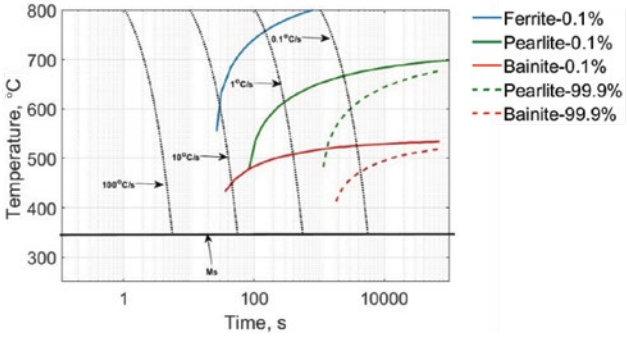

Figure 5

Time-temperature transformation (TTT) plot from JMatPro Simulation (dotted line is representing the variable isothermal holding respectively at 600°C, 550°C, 500°C).

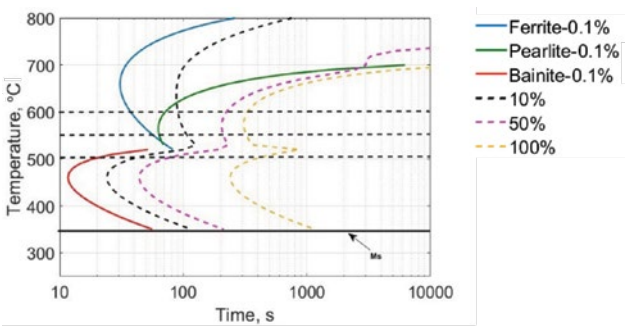

Figure 6

Dilatometric analysis: Example of dilatometric curves of AHSS slab specimen in as-cast condition: Dilatometric curve predicted by JMatPro simulation (a); quenching dilatometric data of each cooling condition (b); and comparison of JMatPro and quenching dilatometric data in 10°C/second (c), 1°C/second (d), and 0.1°C/second (e) cooling conditions.

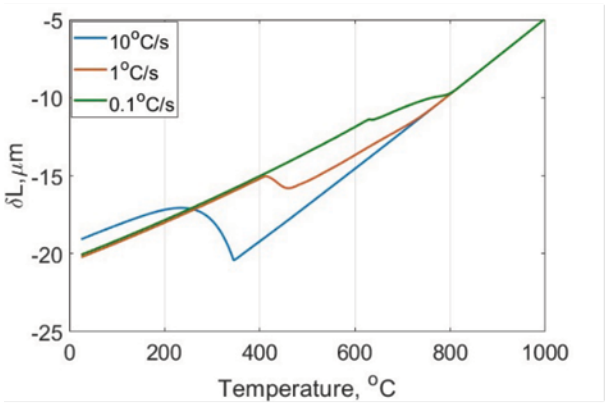

(a)

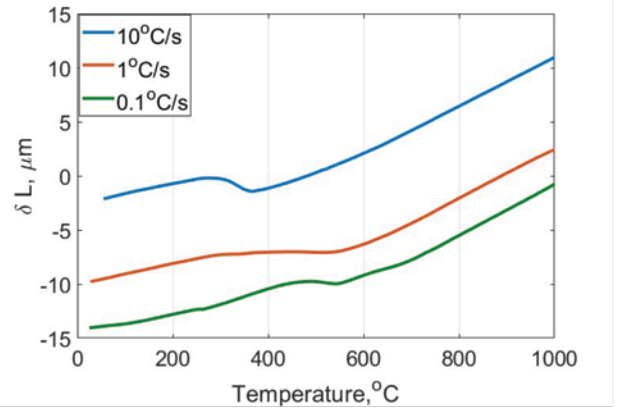

(b)

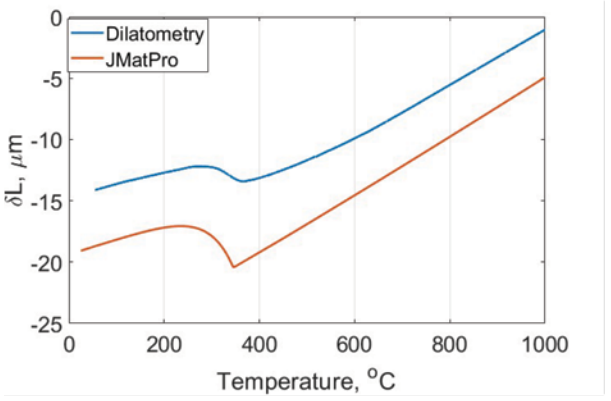

(c)

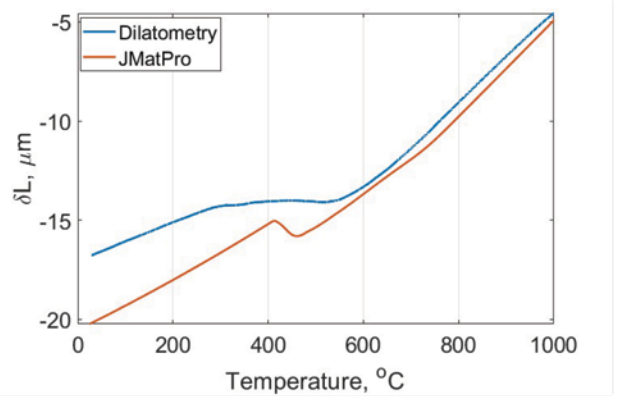

(d)

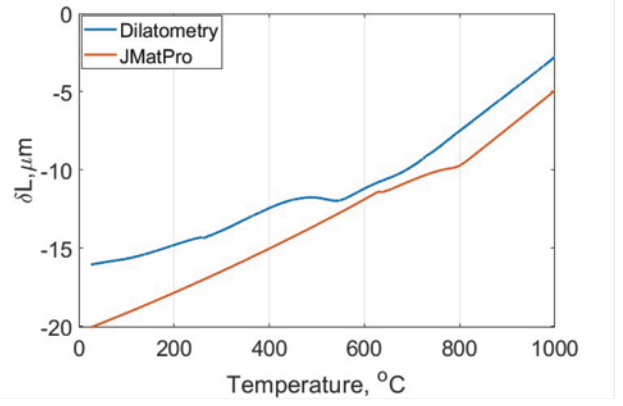

(e)

At the 0.1°C/second condition, JMatPro predicted ferrite formation at a higher temperature (~800°C) than experimental dilatometry (~750°C). Additionally, a small amount of pearlitic transformation was visible in both cases at around 600–630°C. In addition, the bainite transformation was observed at 550°C which was not predicted in simulation. Overall, simulation was not very effective predicting the bainite transformation temperatures in this AHSS grade.

Fig. 7a shows the simulated austenite transformation fraction versus temperature plot in different cooling conditions using JMatPro. 10°C/second showed mostly

Figure 7

Phase transformation: Predicted by JMatPro (a), and experimentally measured using dilatometry (b).

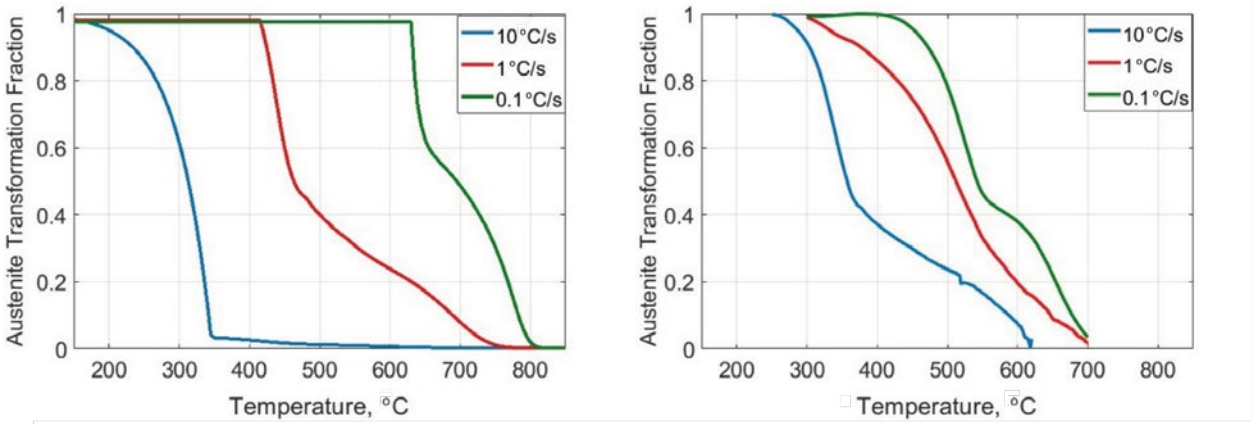

martensitic transformation starting at ~350°C. 1°C/second showed acicular ferrite transformation at ~650°C and bainitic transformation at ~500°C. However, 0.1°C/second showed high temperature polygonal ferrite (PF) at ~750°C and acicular ferrite (AF) at ~650°C.

Fig. 7b shows the experimental phase fraction versus temperature plot, where it was found that an increase of cooling rate shifted the transformation temperature to lower values. the phase transformation curve was plotted using experimental dilatometric data in MATLAB which is described in a previous publication.[13] 10°C/second showed mostly martensitic transformation along with a trace amount of bainite whereas a mixture of ferrite, bainite, and martensite was found in 1°C/second condition. However, 0.1°C/second showed mostly bainitic transformation and ferrite phases (allotriomorphic and acicular).

Microstructure Analysis

As-Cast Condition and Post-Dilatometry: Fig. 8 shows optical microscopic images of industrially processed AHSS in as-cast condition. As-cast micros displayed the mixture of martensite and bainite.

Fig. 9 shows the microstructures captured after quenching dilatometry in 10°C/second cooling condition. 10°C/

Figure 8

As-received microstructures of AHSS specimen in as-cast condition. M: Martensite, B: Bainite using optical microscope (OM), at two different magnifications.

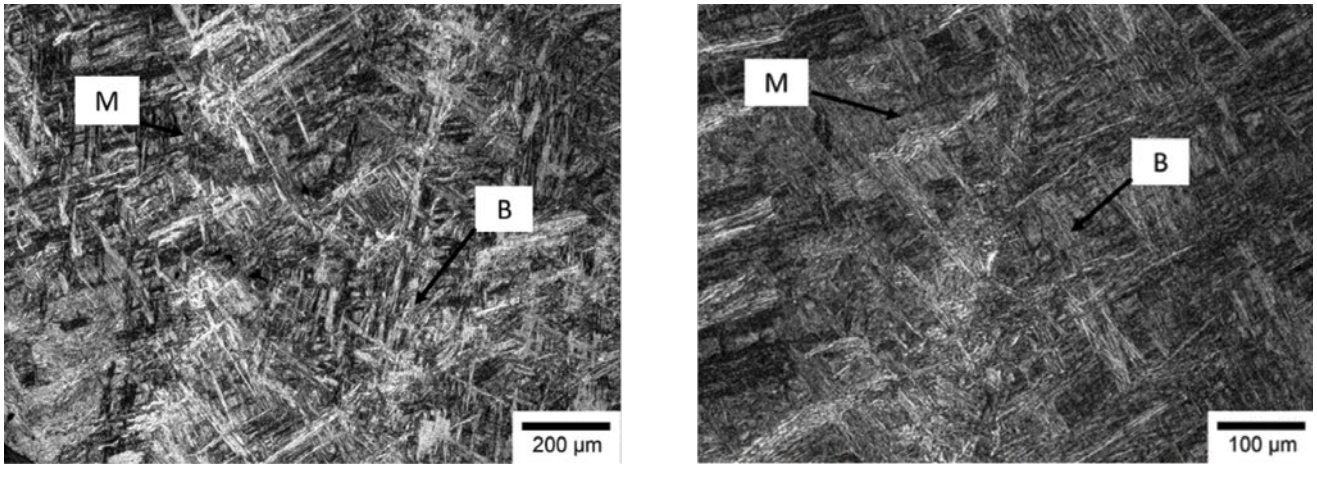

Figure 9

Microstructures of quenching dilatometry specimen in 10°C/second condition using OM, at two different magnifications.

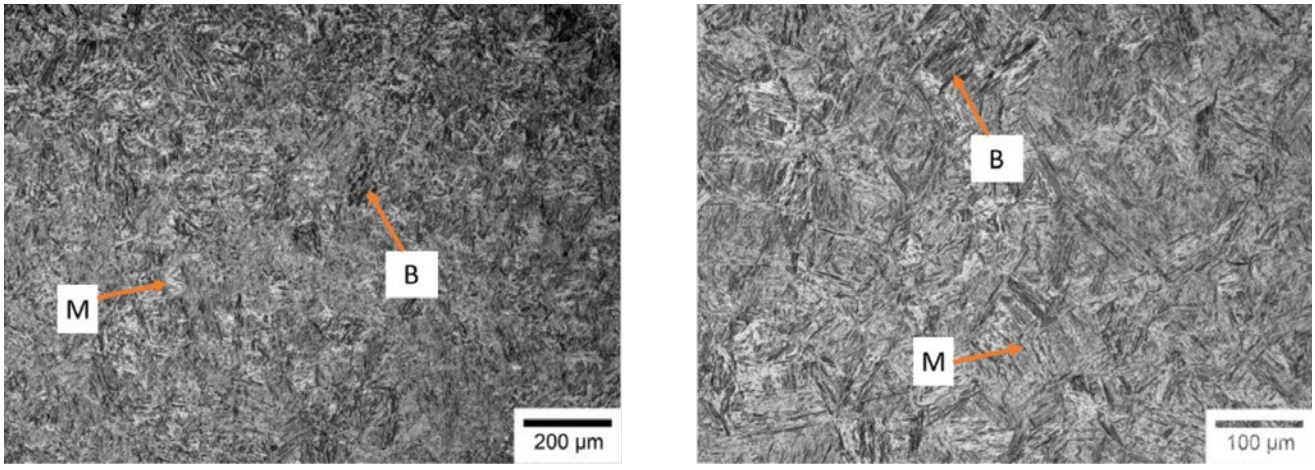

(a) (b)

Figure 10

Microstructures of quenching dilatometry specimen in 1°C/second condition using OM, at two different magnifications.

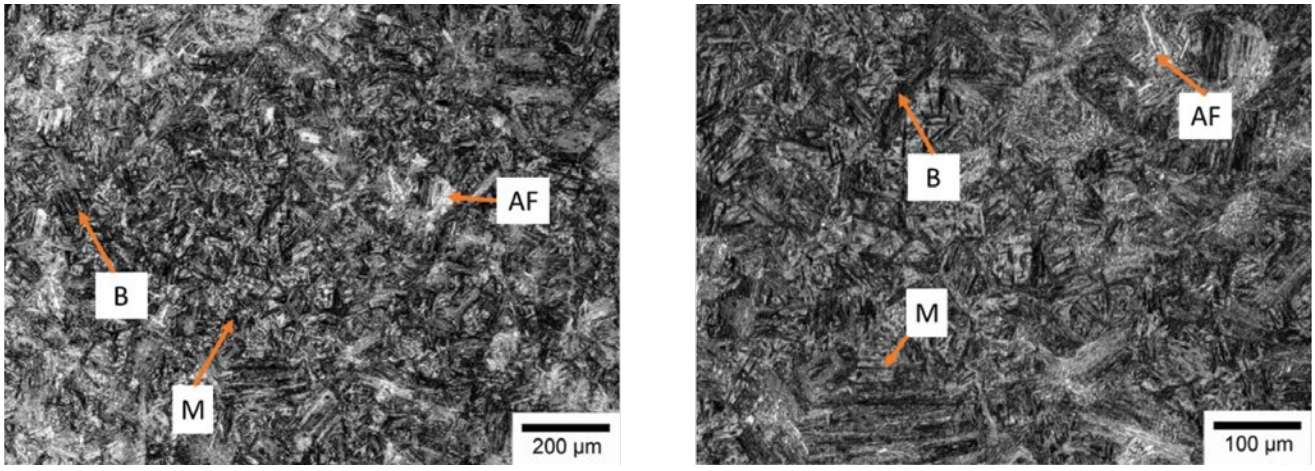

(a) (b)

second micros are comprised with mostly martensite and small portion of bainite.

Fig. 10 shows the microstructure of 1°C/second specimen which is composed of three different phases (ferrite, bainite and martensite). However, the main difference observed from 10°C/second condition is the increased amount of bainite. Since the cooling rate is reduced, acicular ferrite has also started to appear.

Fig. 11 shows the 0.1°C/second specimen, which is made of ferrites (allotriomorphic, acicular) and bainite. Due to the slow cooling rate, high-temperature ferrite such as allotriomorphic or PF along with a higher fraction of AF are observed in the micros. However, bainite is still present in the microstructures in both granular and acicular morphologies. Additionally, even though JMatPro simulation predicted the formation of pearlite in this cooling rate, no pearlite was visible in the microstructures. It can be assumed that a higher Mn, Si content has shifted the pearlite nose right to the CCT diagram therefore, slower cooling rate than 0.1°C/second is required to form pearlite for this steel grade.[4]

Figure 11

Microstructures of quenching dilatometry specimen in 0.1°C/second condition using OM, at two different magnifications.

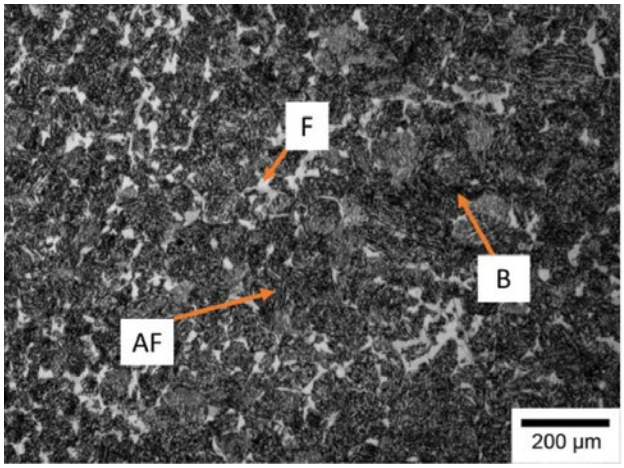

(a)

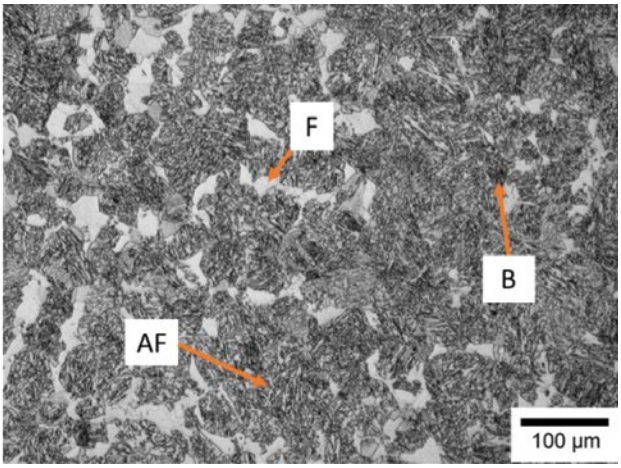

(b)

Figure 12

Microstructure of hot-rolled specimen isothermally held at 600°C for 24 hours; air cooled: OM (a), and scanning electron microscope (SEM) (b).

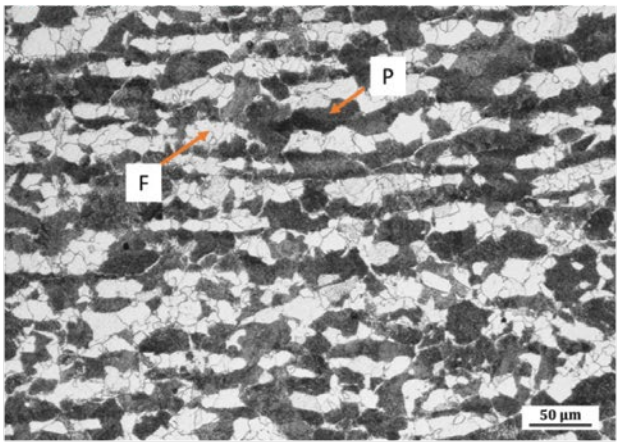

(a)

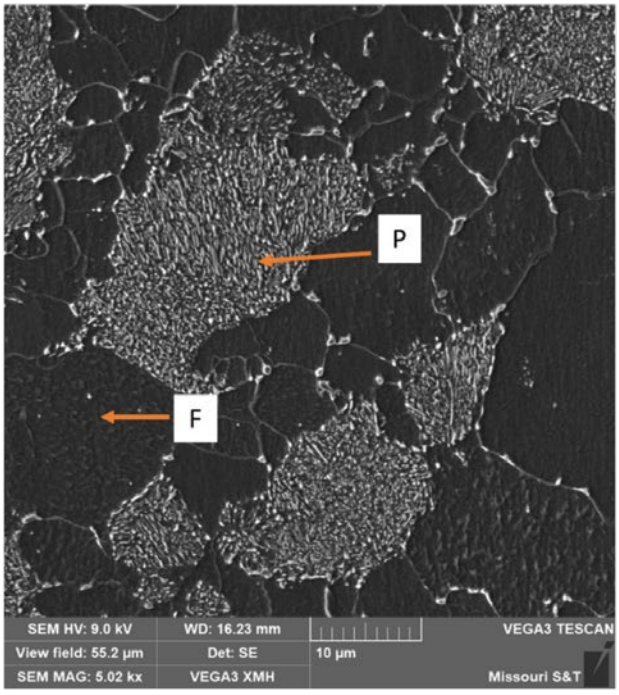

(b)

Figure 13

Microstructure of hot-rolled specimen isothermally held at 550°C for 24 hours; air cooled: OM (a), and SEM (b).

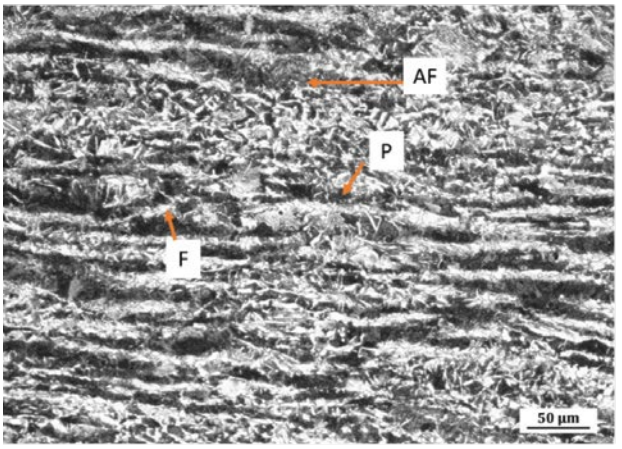

(a)

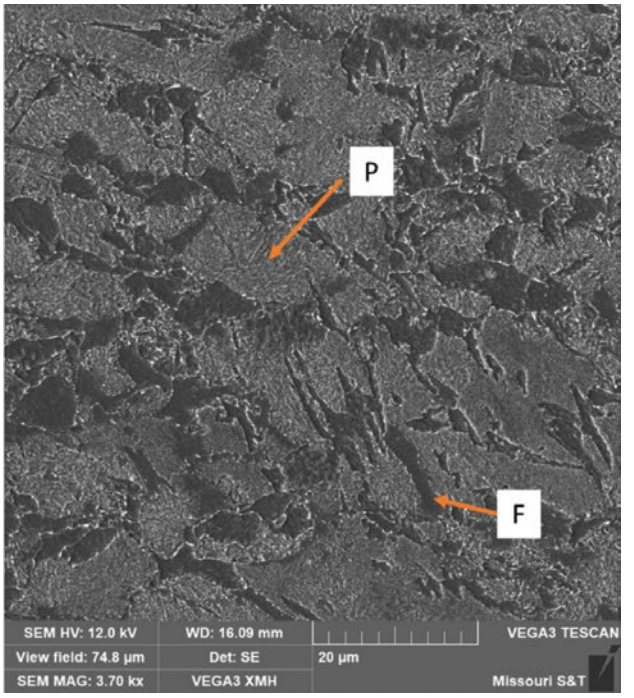

(b)

Comparing as cast microstructure with post-dilatometric micros, it can be inferred that the cooling rate after slab casting was between 1°C/second and 10°C/second. 10°C/second and higher cooling rates generate a mostly martensitic structure. However, the 1°C/second condition showed predominantly bainite, whereas 0.1°C/second showed predominant ferrites.

Hot-Rolled Condition: Fig. 12 shows the microstructure of the hot-rolled specimen after isothermally held at 600°C for 24 hours. Fig. 12a shows the optical microscopy whereas, Fig. 12b the SEM images. A homogeneous mixture of ferrite and pearlite was observed in the micros where pearlite was aligned with the rolling direction. Deformed ferrite resulted from hot rolling was also observed. The TTT diagram in Fig. 5 also predicted a similar ferrite-pearlite morphology. On other hand, Fig. 12b shows the fine lamellar structure of pearlite inside the grain.

Fig. 13 shows the microstructures of the hot-rolled specimen after isothermally held at 550°C for 24 hours. Fig. 13a shows the optical microscopy, whereas Fig. 13b shows the SEM images. Micros of this condition are similar to their 600°C counterparts. Fig. 13a shows mostly ferrite-pearlite structure with smaller pearlite colonies than at 600°C. The higher isothermal holding temperature caused the larger grain size in Fig. 13a. It also shows an acicular/bainitic feature which was not observed in the higher temperature isothermal micros (Fig. 12). The possible reason for having both pearlite and bainite is the isothermal holding at the critical temperature where both pearlite and bainite region overlap. Bainite regions were clearly noticeable in the high magnification SEM images (Fig. 13b).

Fig. 14 shows the microstructures of the hot-rolled specimen after isothermally held at 500°C for 24 hours. Fig. 14a shows the optical microscopy, whereas Fig. 14b shows the SEM images. It was estimated from the CCT and TTT diagram that bainite region started to form below ~550°C. So, a fully bainitic microstructure was predicted in 500°C isothermal condition. Fig. 14a shows the fully bainitic microstructures which are already verified by microhardness testing. Bainite morphology was also clearly visible in the high-magnification images obtained by TESCAN SEM in Fig. 14b.

Mechanical Properties

Hardness Testing: Table 2 shows the result of macrohardness taken in HRB scale which is converted to Vickers Scale (HV), whereas Table 3 shows the result of the microhardness in Vickers Scale (HV).

As-cast condition sample showed macrohardness values 235 HV, which is closer to the 500°C isothermal hold sample (241 HV). However, the high isothermal hold samples (550°C, 600°C) showed lower macrohardness

Figure 14

Microstructure of hot-rolled specimen isothermally held at 500°C for 24 hours; air cooled: OM (a), and SEM (b).

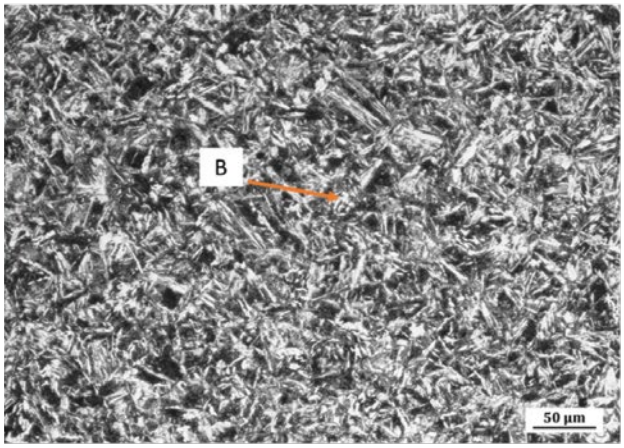

(a)

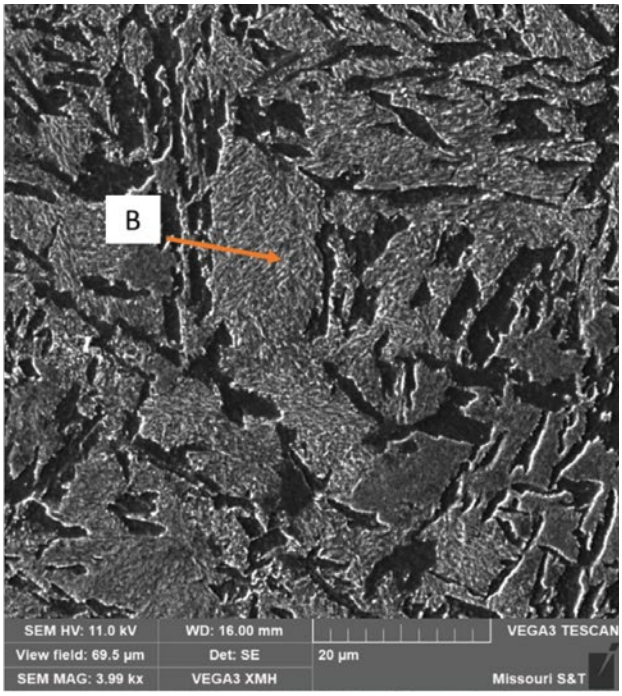

(b)

value than both as-cast and 500°C isothermal hold sample. 550°C isothermally hold sample showed higher Macrohardness (222 HV) than 600°C isothermally hold sample (197 HV).

The lower isothermal hold sample (500°C) showed a higher microhardness value whereas, higher isothermal hold (550°C, 600°C) specimen showed the lowest hardness value and a very different morphology. However, the microhardness data in Table 3 provides the hardness variation based on different phases. According to the different features obtained in OM, the microhardness data identifies the accurate morphology. Both 600°C (Fig. 12) and 550°C (Fig. 13) showed similar macrohardness values (200 HV) but their microhardness data indicates that the white feature in the 600°C sample was softer PF (207 HV), whereas it was bainite in the 550°C sample which had a higher HV value (300). Also, the black region in the 600°C sample was not as hard (270 HV) as the region in 550°C sample, which had higher HV value (350). The difference of these HV values suggests the region in the 600°C sample was pearlitic, while region in the 550°C sample was more bainitic in morphology. Moreover, the 500°C sample (Fig. 14) also exhibited the microhardness in the bainitic range (300-370 HV).

Tensile Testing: Fig. 15 shows the engineering and true stress-strain plot obtained from tensile testing. The as-cast specimen showed the maximum yield strength (YS) (~557 MPa) and ultimate tensile strength (UTS) (~841 MPa) but also the lowest ductility with <10% total elongation and area of reduction. On the other hand, the hot-rolled specimens displayed improved ductility

Table 2

Average Rockwell Macrohardness (HV) Values in Each Condition (As-Cast and Hot-Rolled)

As-Cast	600°C	550°C	500°C
235	197	222	241

Table 3

Average Vickers HV Values in Each Condition (As-Cast and Hot-Rolled)

Feature	As-Cast	600°C	550°C	500°C
White	407	207 (PF)	300 (B)	300 (B)
Black	448	270 (P)	350 (B)	370 (B)

Figure 15

Stress-strain plot obtained from hot-rolled specimen in four conditions. E: Engineering; T: True.

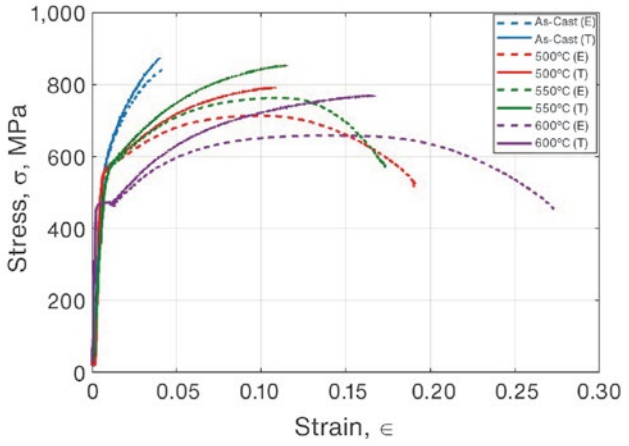

without compromising YS. The sample isothermally held at 500°C showed the maximum YS (~557 MPa) and elongation (24.6%) among hot-rolled conditions. With a decrease of isothermal holding temperature after hot rolling, YS started to decline. The hot-rolled specimen isothermally held at 600°C had the lowest YS (466 MPa) and UTS value (650 MPa) and exhibited highest elongation (~31%).

On the other hand, hot-rolled samples isothermally held at 500°C and 550°C showed similar mechanical properties. Both exhibited 24% elongation and yield strain of ~0.0027. However, the yield strength was found to be slightly higher (~20 MPa difference) in the 500°C sample (558 MPa) than in the 550°C sample (538 MPa). Even though the 500°C specimen exhibited a higher YS, the 550°C sample exhibited a higher UTS value (760 MPa) than the 500°C counterpart (710 MPa). The difference in tempering cycles after hot rolling was found to be responsible for the observed difference in mechanical properties captured in Table 4.

To summarize the tensile results, the fully bainitic morphology of the 500°C condition is responsible for having higher YS than the pearlitic microstructure observed in 600°C. However, a mixture of both bainite and pearlite in the 550°C condition was the reason behind the higher UTS and better ductility for this condition. Even though the as-cast material shows both the highest YS and UTS, the martensitic microstructure made the material less ductile (<10% elongation), which is undesirable for automotive applications.

Conclusion

The current work examined the effect of different tempering temperature after hot rolling of an advanced high-strength steel for automotive applications. After performing lab-scale hot rolling, the effect of tempering temperature on hot-rolled steel was studied using JMatPro simulations, microstructural analysis and mechanical testing. Based on the experimental and simulated data analysis, the following conclusions were found:

- Quenching dilatometry data identified a discrepancy between JMatPro simulation data and experiment at intermediate cooling rate (1°C/second, 0.1°C/second) where two phases coexist in this steel grade.
- Quenching dilatometry shows martensitic micros at 10°C/second, bainitic microstructure at 1°C/second, and bainite along with ferrites (acicular, polygonal) at 0.1°C/second. However, no pearlite was observed even if simulation was predicting it.
- Quenching dilatometry data identified the discrepancy of JMatPro simulation data at an intermediate cooling rate (1°C/second, 0.1°C/second) where two phases coexist in this steel grade.

Table 4

Data Obtained From Tensile Testing

Condition	Elongation, %	Area of reduction, %	Ultimate tensile strength, MPa	Yield strain, mm/mm	Yield stress, MPa
As-cast	7.52	6.00	841	0.0028	557
Hot-rolled, 500°C	24.6	70.3	710	0.0028	558
Hot-rolled, 550°C	24.24	55.4	760	0.0027	538
Hot-rolled, 600°C	30.44	31.81	650	0.0023	466

- As-cast micros were made of martensite and bainite, which gives an idea about the cooling rate being in between 10°C/second and 1°C/second. Despite having highest YS and UTS, it was brittle in nature.
- The hot-rolled specimen which was isothermally hold at 500°C for 24 hours showed the fully bainitic microstructure. It has higher YS than 550°C and 600°C counterparts.
- The hot-rolled specimen which was isothermally held at 550°C for 24 hours showed the mixture of ferrite-bainite-pearlite microstructure, which provides a better combination of high strength and ductility than other conditions.
- The hot-rolled specimen which was isothermally held at 600°C for 24 hours showed the homogeneous ferrite-pearlite morphology, which has the lowest YS and UTS but is ductile in nature.

Acknowledgment

This research was funded by the sponsors of the Peaslee Steel Manufacturing Research Center (PSMRC), and industry/university cooperative research center. The authors are grateful to Thinium Natarajan and Matthew Merwin of U. S. Steel Research and Technology Center for providing the experimental materials.

References

1. J. Galan, L. Samek et al., "Advanced High Strength Steels for Automotive Industry," *Revista De Metallurgia,* Vol. 48, No. 2, 2012, pp. 118–131.
2. C. Lesch, N. Kwiaton et al., "Advanced High Strength Steels (AHSS) for Automotive Applications-Tailored Properties by Smart Microstructural Adjustments," *Steel Research International,* Vol. 88, No. 10, 2017, pp. 1–21.
3. R. Kuziak, R. Kawalla et al., "Advanced High Strength Steels for Automotive Industry," *Archives of Civil and Mechanical Engineering,* Vol. 8, 2008, pp. 103–117.
4. M. Breuer, M. Degner et al., "Influence of Cold Rolling on the Mechanical and Technological Properties of AHSS Steel Grades," *Seminario de Laminacao e Conformacao de Metals,* Vol. 54, No. 1, 2017, pp. 28–39.
5. H.K.D.H. Bhadeshia and R. Honeycomb, *Steels Microstructure and Properties,* 3rd Ed., Elsevier, 2006.
6. G. Krauss, *Steel: Processing, Structure, and Performance,* 2nd Ed., ASM International, 2015.
7. A. Smith, F. Vercruysee et al., "The Effect of Niobium on Austenite Evolution During Hot Rolling of Advanced High Strength Steel," *Journal of Physics: Conference Series,* Vol. 1270, 2019, pp. 1–7.
8. K. Li, J. Shao et al., "Effect of Nb-Ti Microalloyed Steel Precipitation Behavior on Hot Rolling Strip Shape and FEM Simulation," *Materials,* Vol. 17, No. 3, 2024, p. 651.
9. T. Kvackaj, J. Bidulska et al., "Overview of HSS Steel Grades Development and Study of Reheating Condition Effects on Austenite Grain Size Changes," *Materials,* Vol. 14, No. 8, 1988.
10. W. Bleck, F. Bruhl et al., "Materials and Processes for the Third-Generation Advanced High-Strength Steels," *Berg Huettenmaenn Monatsh,* Vol. 164, No. 11, 2019, pp. 466–474.
11. O.N. Cora and M. Koc, "Promises and Problems of Ultra/Advanced High Strength Steel (U/AHSS) Utilization in Automotive Industry," *7th Automotive Technologies Congress,* 2014.
12. D. Casellas, A. Lara et al., "Fracture Toughness to Understand Stretch-Flangeability and Edge Cracking Resistance in AHSS," *Metallurgical and Materials Transactions A,* Vol. 48A, 2017, pp. 86–94.
13. B. Saha, H. Haffner et al., "Effect of Ti on Phase Transformation and Grain Evolution in Nb/V Microalloyed Steel," *AISTech 2024 Conference Proceedings,* 2024, pp. 1697–1705.

This paper was presented at AISTech 2025 — The Iron & Steel Technology Conference and Exposition, Nashville, Tenn., USA, and published in the AISTech 2025 Conference Proceedings.